Journal of Alloys and Compounds 696 (2017) 1019–1030

Contents lists available at ScienceDirect

Journal of Alloys and Compounds

journal homepage: http://www.elsevier.com/locate/jalcom

The ternary system cerium–iridium–silicon

Alexey Lipatov [a, b, *], Alexander Gribanov [c], Sergey Dunaev [c]

[a] Department of Chemistry, University of Nebraska – Lincoln, Lincoln, NE 68505, United States
[b] Department of Materials Science, Moscow State University, Leninskie Gory, GSP-1, 119991 Moscow, Russia
[c] Department of Chemistry, Moscow State University, Leninskie Gory, GSP-1, 119991 Moscow, Russia

ARTICLE INFO

Article history:
Received 4 October 2016
Received in revised form
28 November 2016
Accepted 1 December 2016
Available online 2 December 2016

Keywords:
Intermetallics
Metals and alloys
Phase diagrams
Crystal structure
Scanning electron microscopy
X-ray diffraction

ABSTRACT

Phase relations in the ternary system Ce–Ir–Si have been established and the isothermal section at 950 °C was constructed based on X-ray powder diffraction, scanning electron microscopy, and electron probe microanalysis techniques on 83 alloys, which were prepared by arc melting under argon or powder reaction sintering. Among the 15 ternary compounds observed at 950 °C 8 phases have been reported earlier. Based on powder X-ray diffraction data the crystal structures for 6 new ternary phases were assigned to known structure types: τ_6 – Ce_3IrSi_3 (Ta_3B_4-type), τ_8 – $Ce_3Ir_4Si_4$ ($U_3Ni_4Si_4$-type), τ_{10} – $Ce_6Ir_{30}Si_{19}$ ($Sc_6Co_{30}Si_{19}$-type), τ_{12} – $Ce_2Ir_{12}Si_7$ ($Ho_2Rh_{12}As_7$-type), τ_{13} – $Ce_3Ir_{2-x}Si_{2+x}$ ($Sm_3Ir_2Si_2$-type), and τ_{14} – $Ce_3Ir_3Si_2$ ($Ce_3Rh_3Si_2$-type). For another new compound τ_1 – $Ce_4Ir_{27}Si_{69}$ (at.%), which has homogeneity region along 27 at.% of Ir, the reflections were indexed in hexagonal lattice symmetry with cell parameters close to high-temperature $IrSi_{3-x}$ phase.

1. Introduction

Intermetallic compounds formed by transition metals with itinerant *d*-electrons and Rare Earth metals with more localized *f*-electrons exhibit a wide variety of unusual physical properties. Effects such as mixed and intermediate valence states, heavy fermion and non-Fermi liquid behaviors, unconventional superconductivity, Kondo-lattices and Kondo-semiconductors, quantum criticalities, *etc.* were among the central topics in solid-state chemistry and physics for decades [1]. Unconventional behavior of this family of compounds originates from the hybridization effect between *f*-electrons of Rare Earth atoms and conduction electrons on Fermi level leading to the strong electronic correlations. So far, there is no good general approach for understanding these strongly correlated systems. Synthesis of new *f*-electron materials and the subsequent experimental measurements of their electrical and magnetic properties can lead to new insights into interaction between electrons and magnetic spins of Rare Earth metals.

Ternary systems R-T-X consisted of Rare Earth metal (R), transition *d*-element (T) and element of 13–14 groups (X) proved to be a rich source of compounds demonstrating strongly correlated electron behavior. Among known variety of this family compounds the most outstanding are $CeCu_2Si_2$, $YbRh_2Si_2$, $CePd_2Si_2$, $CeNi_2Ge_2$, $CeRu_2Si_2$, $CeRh_2Si_2$, $CeCoIn_5$, $CePt_3Si$, which have been described in many papers and reviews (see for instance, [2–6]) Another important feature of R-T-X ternary systems is a rich and diverse crystal chemistry of its intermetallic compounds. In the nearest analogous to the titled Ce–Ir–Si system, Ce–Pt–Si, Ce–Pd–Si and Ce–Rh–Si systems, 19, 21 and 27 ternary compounds, correspondingly, were recently detected [7–9]. Due to a large number of formed compounds, studying R-T-X ternary systems is a promising area of search for new compounds with unconventional electronic properties.

Typically, known compounds in the R-T-X systems belong to a number of selected series, such as RTX, RTX_2, RTX_3, RTX_5, RT_2X_2, R_2TX_3, $R_2T_3X_5$, RT_3X. Unconventional electronic properties of the series prototype stimulate investigation of new compounds with the same composition but different elements (for instance $CeCu_2Si_2$ [10] for RT_2X_2 series [11], $CeCoIn_5$ [12] for RTX_5 series [13,14], $CePt_3Si$ [15] for RT_3X series [16]). As a result, for many ternary systems several compounds were reported, but the entire system is not investigated. Meanwhile, there are a lot more compounds formed in R-T-X systems, and more systematic search for new compounds is required. In the mentioned above Ce–Pt–Si, Ce–Pd–Si and Ce–Rh–Si systems, 7, 8 and 11 novel ternary compounds, respectively, were detected in our previous investigations

* Corresponding author. Department of Chemistry, University of Nebraska – Lincoln, Lincoln, NE 68505, United States.
E-mail address: avlipatov@gmail.com (A. Lipatov).

http://dx.doi.org/10.1016/j.jallcom.2016.12.014
0925-8388/

[7–9].

Studies of the next similar ternary system – Ce–Ir–Si – had been performed on the individual compounds, but it is unclear whether all the intermetallic compounds were found. We have performed the investigation of the Ce–Ir–Si system in the full range of concentrations and report the results in this paper. We revealed the formation of 7 new intermetallics and established equilibrium states in isothermal section of Ce–Ir–Si system at 950 °C. We also confirmed the formation and structure of eight ternary compounds in the system: $CeIrSi_3$ ($BaNiSn_3$-type [17,18], $CeIrSi_2$ ($CeNiSi_2$-type) [19], $Ce_2Ir_3Si_5$ ($U_2Co_3Si_5$-type) [20], CeIrSi (LaIrSi-type) [21], $CeIr_2Si_2$ (α and β forms, $ThCr_2Si_2$- and $CaBe_2Ge_2$-types, correspondingly [22,23]), $CeIr_{2-x}Si_{1+x}$ ($CeIr_2Si$-type) [24], Ce_2IrSi_3 (Ce_2CoSi_3-type) [25], and $CeIr_3Si_2$ ($ErRh_3Si_2$-type) [26,27].

For seven compounds, physical properties were reported earlier. $CeIrSi_3$ is a pressure-induced heavy-fermion noncentrosymmetric superconductor (see, for instance, [28–31]). $CeIrSi_2$ [19,32] and both α and β modifications of $CeIr_2Si_2$ [33] demonstrate valence instabilities of Ce-atoms. Similarly, for $Ce_2Ir_3Si_5$ compound small charge fluctuations of Ce atoms were reported [34,35]. Antiferromagnetic ordering below 1.3 K with metamagnetic-like phase transition in 5 kOe applied field were detected for Ce_2IrSi_3 [25,36]. $CeIr_3Si_2$ reveals long-time variation of magnetic structure, successive magnetic transitions in zero magnetic field and multi-step metamagnetic transitions at relatively low magnetic field [26,27,37,38]. CeIrSi is a Curie-Weiss paramagnetic above 100 K with an experimental magnetic moment of 2.56 μ_B/Ce-atom [21]. No data on the physical properties of $CeIr_{2-x}Si_{1+x}$ were published hitherto. Further investigation of Ce–Ir–Si in the entire concentration range may reveal new compounds exhibiting unconventional electronic properties.

2. Experimental techniques

A total of 83 alloys were synthesized in this work from high purity elements. Starting metals Ir (99.997 mass %, Krasnoyarsk, Russia) and Si (99.9999 mass %, Usolie-Sibirskoe, Russia) were used as received. In order to remove oxides from the surface of the Ce (electrolytic, 99.95 mass %, Novosibirsk, Russia), the precursor was cleaned by metal file no later than 30 min prior to synthesis. The starting materials were weighed on analytical balances to ±0.0001 g in the exact proportion corresponding to molar composition of an alloy. A typical mass of a sample was 1 g. The alloys were prepared by arc-melting in a compact Arc Melter MAM-1 furnace (Edmund Bühler Gmbh, Hechingen, Germany) performed on a water-cooled copper hearth under argon atmosphere. To ensure homogenization, all samples were turned over and melted three times. Part of each sample was vacuum-sealed in a quartz tube and annealed at 950 °C for 30 days before being quenched in cold water. If an alloy did not achieve homogenization after 30 days (more than 3 phases detected), it was powdered in mortar, cold compacted to a tablet and sintered at 950 °C for an additional week in a vacuum-sealed quartz tube. In the latter case, only X-ray powder diffraction (XPD) data were used to identify the compounds which form an equilibrium state. Electron probe microanalysis (EPMA) and XPD tests did not reveal oxygen and oxides in the prepared alloys or powders.

XPD data of as-cast and annealed samples were collected using a monochromatic Cu-$K_{\alpha 1}$ radiation (λ = 0.15406 nm) on a STOE STADI P transmission diffractometer equipped with a linear position sensitive area detector (STOE & Cie Gmbh, Darmstadt, Germany; step size 0.01°, measurement time 10 s/point, divergence slit 0.3). XPD peaks indexing and the lattice parameters calculations were performed with the STOE WinXpow program package [39]. Quantitative Rietveld refinements of the powder XPD patterns were performed with the FULLPROF program [40,41], employing internal tables for X-ray atomic form factors. Starting atomic parameters for prototypes were taken from a Landolt-Börnstein Database (on-line web-site [42]).

Each sample was prepared via standard technique and examined by scanning electron microscopy (SEM) on a LEO EVO 50XVP instrument (Carl Zeiss, Oberkochen, Germany). Phase compositions were determined via electron probe microanalysis (EPMA) using Link EDX INCA Energy 450 system (Q-BSD detector). The average accuracy in determining the chemical composition was 0.9 at.%.

3. Binary systems

The latest version of the Ce–Ir binary system was reported by Okamoto [43] as a review based on the earlier works [44–47]. Ce–Si phase diagram was adopted from an investigation by Bulanova et al. [48] amended by Ce_2Si_{3-x} (x = 0.32) phase reported in Ref. [49]. Ir-Si phase diagram was taken from two reviews of Okamoto [50,51]. The final version [51] compiles two diagrams: silicon-rich part from 50 to 100 at. % Si by Ref. [52], and iridium-rich part from 0 to 50 at.% Si by Ref. [53]. According to previous findings [54], the binary compound with highest concentration of Si exists in two polymorphic modifications and its chemical composition differs from the exact stoichiometry 1:3 (in Ref. [54] purest phase was found in a sample of composition $Ir_{26}Si_{74}$ (at.%) – so, in our work we call it $IrSi_{3-x}$. The crystal structure of the high temperature polymorphic modification of $\beta IrSi_{3-x}$ is reported in two versions. At first it was determined as hexagonal structure by both XPD [55–57] and single crystal X-ray diffraction methods [58]. Later, based on a new XPD experiment on a modern equipment, Engström et al. [54] revised the crystal structure of $\beta IrSi_{3-x}$ and proposed a lower symmetry orthorhombic structure with cell parameters $a = 0.75634$, $b = 0.43469$, and $c = 0.66238$ nm, which are closely related to previously reported parameters of hexagonal $\beta IrSi_{3-x}$ [54]. The crystal symmetry of a room temperature phase $\alpha IrSi_{3-x}$ was defined as slightly monoclinically distorted relative of the orthorhombic $\beta IrSi_{3-x}$ with lattice parameters $a = 0.76976$, $b = 0.43770$, $c = 0.65467$ nm, and monoclinic angle $\beta = 91.594°$ [54]. However, the atomic orders of both orthorhombic and monoclinic unit cells were not determined.

Crystallographic data of unary and binary phases related to the Ce–Ir–Si ternary system are summarized in Table 1 together with the crystal structures of ternary compounds.

4. Results and discussion

4.1. Phase relations; the isothermal section Ce–Ir–Si at 950 °C

The isothermal section Ce–Ir–Si at 950 °C is presented in Fig. 1. The selected temperature was higher than the melting point of Ce, which resulted in liquid phase formation (marked by wavy line) at 950 °C around Ce corner of the diagram. The present study revealed the formation of 15 ternary intermetallics in the Ce–Ir–Si system at 950 °C. Eight of them, reported earlier and listed in the introduction of this paper, have been confirmed and seven new ternaries have been detected in the present work. Phase relations in the ternary system at 950 °C (Fig. 1) are characterized by the absence of cerium solubility in the iridium silicides due to significantly larger atomic radius of cerium (0.183 nm [59]) compared to radii of Ir and Si atoms (0.136 nm and 0.133 nm, respectively [59]). Close dimensions of iridium and silicon atoms, on the other hand, give a potential for their mutual substitution in crystal structures of five binary ($CeSi_{2-x}$, Ce_5Si_4, Ce_3Si_2, Ce_5Si_3, and $CeIr_2$) and six ternary compounds ($\tau_3 - Ce_2Ir_{1-x}Si_{3+x}$; $\tau_4 - CeIr_{1-x}Si_{2+x}$; $\tau_9 - CeIr_{1-x}Si_{1+x}$; $\tau_{11} - CeIr_{3-x}Si_{2+x}$; $\tau_{13} - Ce_3Ir_{2-x}Si_{2+x}$; and $\tau_{15} - CeIr_{2-x}Si_{1+x}$)

Table 1
Crystallographic data of solid phases in the Ce–Ir–Si system.

Phase/Temperature range (°C)	Space group, Prototype	Lattice parameters, nm			Comments[a]
		a	*b*	*c*	
Unary compounds					
(δCe) 798–726 [64]	$Im\bar{3}\,m$, W	0.412			[64]
(γCe) 726–61 [64]	$Fm\bar{3}m$, Cu	0.51610			[64]
(βCe) 61 – (−177) [64]	$P6_3/mmc$, αLa	0.36810		1.1857	[64]
(αCe) < −177 [64]	$Fm\bar{3}m$, Cu	0.485			[64]
(Ir) < 2447 [64]	$Fm\bar{3}m$, Cu	0.38393			[65]
(Si) < 1414 [64]	$Fd\bar{3}m$, C (diamond)	0.54306			[64]
Binary compounds					
Ce_5Si_3 < 1260 [48]	$I4/mcm$, Cr_5B_3	0.7896		1.3722	[66]
		0.785		1.372	[67]
		0.7878		1.367	[48]
$Ce_5Ir_xSi_{3-x}$					$0 \le x \le 0.5$ [TW][b]
		0.78727(7)		1.37935(9)	x = 0.5 [TW]
Ce_3Si_2 < 1335 [48]	$P4/mbm$, U_3Si_2	0.7800		0.4365	[66]
		0.7780		0.4367	[48]
$Ce_3Ir_xSi_{2-x}$					$0 \le x \le 0.1$ [TW]
		0.77764(8)		0.43654(3)	x = 0.1 [TW]
Ce_5Si_4 < 1500 [48]	$P4_12_12$, Zr_5Si_4	0.7920		1.499	[67]
		0.7949		1.5069	[66]
		0.7936		1.5029	[48]
$Ce_5Ir_xSi_{4-x}$					$0 \le x \le 0.2$ [TW]
		0.79369(6)		1.5019(5)	x = 0.2 [TW]
CeSi < 1630 [48]	$Pnma$, FeB	0.8295	0.3975	0.5970	[67]
		0.8302	0.3965	0.5967	[66]
		0.8298	0.3961	0.5959	[48]
		0.82998(9)	0.39630(5)	0.59627(7)	[TW]
$CeSi_{1.34}$ (Ce_2Si_{3-x})	$Cmcm$, V_2B_3 (Nd_2Si_{3-x})				In Ref. [49] was obtained after annealing at 1100 °C during two weeks at 35 K [49]
		0.44035	2.48389	0.39517	
>950 [TW]					[TW]: trace amount was detected by EPMA after annealing at 950 °C (see Fig. 2a)
$CeSi_{1.67}$ < 1725 [48]	$Imma$, $GdSi_{2-x}$	0.4123	0.4195	1.3905	[66]
		0.4105	0.4183	1.3912	[48]
		0.41220(2)	0.41913(2)	1.3914(6)	[TW]
$CeSi_{2-x}$ < 1575 [48]	$I4_1/amd$, αThSi$_2$				$0 \le x \le 0.1$ [48]
		0.4192		1.3913	x = 0 [48]
$CeIr_ySi_{2-y}$					$0 \le y \le 0.24$ [TW]
		0.41911(1)		1.39706(6)	x = 0, y = 0 [TW]
		0.41866(3)		1.3995(3)	x = 0, y = 0.17 [TW]
		0.41730(3)		1.4066(2)	x = 0, y = 0.24 [TW]
$Ce_4Ir \le 710$ [43]	unknown	unknown	unknown	unknown	[43], [TW]: not involved in the phase equilibria at 950 °C
$Ce_3Ir \le 880$ [43]	$Pnma$, Fe_3C	0.7232	1.0057	0.6524	[46] [TW]: not involved in the phase equilibria at 950 °C
$Ce_7Ir_3 \le 950$ [43]	$P6_3mc$, Th_7Fe_3	1.0054		0.6325	[45]
		1.0068		0.6323	[46] [TW]: was not detected at 950 °C
$Ce_5Ir_3 \le 1100$ [43]	$P4/ncc$, Pu_5Rh_3	1.1267		0.6367	[47]
		1.1251		0.6371	[46]
		1.12705(7)		0.63682(3)	[TW]
$Ce_5Ir_4 \le 1180$ [43]	$Pnma$, Sm_5Ge_4	0.7420	1.483	0.7640	[68]
		0.7436	1.4776	0.7626	[47]
		0.7442	1.4768	0.7634	[46]
		0.74372(5)	1.47803(9)	0.76261(5)	[TW]
$CeIr_{2+x} \le 2250$ [43]	$Fd\bar{3}m$, $MgCu_2$				$-0.30 \le x \le 0.30$ [42]
		0.7578			[46]
		0.7581			[43]
$CeIr_{2-y}Si_y$ [TW]					$0 \le y \le 0.36$ [TW]
		0.75783(5)			y = 0.08 [TW]
		0.75644(4)			y = 0.18 [TW]
		0.75492(6)			y = 0.26 [TW]
		0.75480(7)			y = 0.36 [TW]
$CeIr_3 \le 2100$ [43]	$R\bar{3}\,m$, $PuNi_3$	0.5288		2.618	[69]
		0.5312		2.6058	[46]
		0.5290		2.6220	[70]
		0.52920(2)		2.6199(8)	[TW]
$Ce_2Ir_7 \le 2000$ [43]	$R\bar{3}\,m$, Gd_2Co_7	0.5284		3.880	[44]
		0.5294		3.8938	[46]
		0.52943(6)		3.9011(8)	[TW]

(*continued on next page*)

Table 1 (*continued*)

Phase/Temperature range (°C)	Space group, Prototype	Lattice parameters, nm			Comments[a]
		a	*b*	*c*	
$CeIr_5 \leq 1950$ [43]	*P*6/*mmm*, $CaCu_5$	0.5282		0.4328	[46]
		0.5298(2)		0.4260(1)	[TW]
	*F*4$\bar{3}$*m*, $AuBe_5$	0.7510			[69]
$Ir_3Si \leq 1545$ [51]	*I*4/*mcm*, Ir_3Si	0.5222		0.7954	[71]
		0.5232		0.7973	[72]
		0.52235(5)		0.79601(8)	[TW]
Ir_2Si 1267–1452 [51]	*Pnma*, βCo_2Si	0.5284	0.3989	0.7615	[73]
					[TW]: not involved in the phase equilibria at 950 °C
$Ir_{1.5}Si \leq 1430$ [53]	*P*6$_3$/*mmc*, Ni_2In	0.3963		0.5126	[55]
		0.39649(2)		0.51229(3)	[TW]
$IrSi \leq 1707$ [51]	*Pnma*, FeAs	0.55579	0.32213	0.62673	[57]
		0.5555	0.3215	0.6267	[52]
		0.55577(3)	0.32147(1)	0.62703(4)	[TW]
$Ir_4Si_5 \leq 1315$ [51]	*P*2$_1$/*m*, Rh_4Si_5	0.58805	0.36181 β = 100.14°	1.2359	[57]
		0.58814(3)	0.36193(1) β = 100.13(1)°	1.2352(1)	[TW]
$Ir_3Si_4 \leq 1408$ [51]	*Pnma*, Rh_3Si_4	1.88741	0.36979	0.57717	[57]
		1.8873(3)	0.36960(1)	0.57722(3)	[TW]
$Ir_3Si_5 \leq 1402$ [51]	*P*2$_1$/*c*, Ir_3Si_5	0.64060	1.4162 β = 116.69°	1.1553	[74]
		0.63994(4)	1.41455(9) β = 116.65(1)°	1.15515(7)	[TW]
$\beta IrSi_{3-x}$ 975–1260 [51]	*P*6$_3$*mc*, $IrSi_3$	0.4350		0.6610	[55]
		0.4350		0.6630	[56]
		0.43538		0.66277	[57]
		0.4351		0.6622	[58]
	orthorhombic, *oS*	0.75634	0.43469	0.66238	[54]
		0.75574(3)	0.43443(1)	0.66234(3)	x = 0.25 [TW], as-cast sample $Ir_{25}Si_{75}$ (at.%)
$\alpha IrSi_{3-x} \leq 975$ [51]	monoclinic, *m*	0.76976	0.43770 β = 91.594°	0.65467	[54]
		0.76903(2)	0.43724(1) β = 91.60(2)°	0.65400(2)	x = 0.25 [TW], annealed $Ir_{25}Si_{75}$ (at.%)
Ternary compounds					
τ_1, ~$Ce_{4\div6}Ir_{27}Si_{69\div67}$ (at.%)	Hexagonal	0.44329(7)		0.65788(7)	[TW], at $Ce_4Ir_{27}Si_{69}$ composition (at.%)
		0.44394(8)		0.65948(9)	[TW], at $Ce_6Ir_{27}Si_{67}$ composition (at.%)
τ_2, $CeIrSi_3$	*I*4*mm*, $BaNiSn_3$	0.4252		0.9715	[18]
		0.42424(2)		0.97924(5)	[TW]
τ_3, Ce_2IrSi_3 $Ce_2Ir_{1-x}Si_{3+x}$	*P*6/*mmm*, Ce_2CoSi_3	0.82120		0.42374	[25] $0 \leq x \leq 0.30$ [TW]
		0.82134(5)		0.42354(2)	$x_{min} = 0$ [TW]
		0.81770(10)		0.42686(4)	$x_{max} = 0.30$ [TW]
τ_4, $CeIrSi_2$ $CeIr_{1-x}Si_{2+x}$	*Cmcm*, $CeNiSi_2$	0.42580	1.6754	0.41917	[19] $0 \leq x \leq 0.16$ [TW]
		0.42533(2)	1.6745(1)	0.41964(2)	$x_{min} = 0$ [TW]
		0.42528(2)	1.6736(1)	0.41945(2)	$x_{max} = 0.16$ [TW]
τ_5, $Ce_2Ir_3Si_5$	*Ibam*, $U_2Co_3Si_5$	0.9953	1.181	0.5804	[20]
		0.99584(5)	1.15670(9)	0.58756(3)	[TW]
τ_6, Ce_3IrSi_3	*Immm*, Ta_3B_4	0.41323(1)	0.42755(1)	1.8182(1)	[TW]
τ_7, $\beta CeIr_2Si_2$	*P*4/*nmm*, $CaBe_2Ge_2$	0.41431		0.98460	[22]
		0.41460		0.9855	[23]
		0.41392(2)		0.98538(5)	[TW]
τ_7, $\alpha CeIr_2Si_2 \leq 920$ [20]	*I*4/*mmm*, $ThCr_2Si_2$	0.40848		1.01583	[22]
		0.40882		1.01696	[23]
τ_8, $Ce_3Ir_4Si_4$	*Immm*, $U_3Ni_4Si_4$	0.40241(2)	0.41430(2)	2.4345(1)	[TW]
τ_9, $CeIr_{1-x}Si_{1+x}$	*P*2$_1$3, LaIrSi				$0.0 \leq x \leq 0.05$ [TW]
		0.62915			$x_{min} = 0.0$ [21]
		0.62757(5)			$x_{min} = 0.0$ [TW]
		0.62709(4)			$x_{max} = 0.05$ [TW]
τ_{10}, $Ce_6Ir_{30}Si_{19}$	*P*6$_3$/*m* $Sc_6Co_{30}Si_{19}$	1.57154(3)		0.38915(1)	[TW]
τ_{11}, $CeIr_{3-x}Si_{2+x}$	*Imma*, $ErRh_3Si_2$	0.71838	0.97373	0.56018	[75]
		0.71768	0.97273	0.55971	[26]
		0.7178	0.9726	0.5597	[27]
					$-0.15 \leq x \leq 0.06$ [TW]
		0.71769(5)	0.97312(7)	0.55974(5)	$x_{min} = -0.15$ [TW]
		0.71801(4)	0.97271(5)	0.55928(4)	x = 0.0 [TW]
		0.71819(5)	0.97263(8)	0.55932(4)	$x_{max} = 0.06$ [TW]
τ_{12}, $Ce_2Ir_{12}Si_7$	*P*6$_3$/*m*, $Ho_2Rh_{12}As_7$	0.97330(4)		0.38664(2)	[TW]

Table 1 (*continued*)

Phase/Temperature range (°C)	Space group, Prototype	Lattice parameters, nm			Comments[a]
		a	*b*	*c*	
τ_{13}, $Ce_3Ir_{2-x}Si_{2+x}$	*Cmcm*, $Sm_3Ir_2Si_2$				$0.0 \le x \le 0.2$ [TW]
		0.41178(2)	1.08136(4)	1.33775(6)	$x_{min} = 0.0$ [TW]
		0.41123(4)	1.08200(7)	1.33804(9)	$x_{max} = 0.2$ [TW]
τ_{14}, $Ce_3Ir_3Si_2$	*Pnma*, $Ce_3Rh_3Si_2$	0.76950(2)	1.48111(4)	0.57065(2)	[TW]
τ_{15}, $CeIr_2Si$	$I4_1/amd$,	0.40698		3.54085	[24]
$CeIr_{2-x}Si_{1+x}$	$CeIr_2Si$				$0.0 \le x \le 0.08$ [TW]
		0.40603(4)		3.5397(3)	$x_{min} = 0.0$ [TW]
		0.40665(2)		3.5322(2)	$x_{max} = 0.08$ [TW]

[a] With an abundance of literary references the authors brought only the selected links; others can be found in the databases such as the Springer Materials [42], and similar.
[b] [TW] – this work.

resulting in the extended (Ce_5Si_3, $CeSi_{2-x}$, $CeIr_2$, τ_3, τ_4, τ_{11}) or at least notable (Ce_3Si_2, Ce_5Si_4, τ_9, τ_{13}, τ_{15}) homogeneous regions. The only exception is a new ternary compound τ_1 – $Ce_4Ir_{27}Si_{69}$ (at. %), which has a homogeneity region along iridium iso-concentrate line of ~27.0 at. %. This unexpected phenomenon was registered by XPD and EPMA techniques, and the obtained experimental data are presented and discussed below. Ternary phases τ_2 – $CeIrSi_3$, τ_5 – $Ce_2Ir_3Si_5$, τ_6 – Ce_3IrSi_3, τ_7 – $CeIr_2Si_2$, τ_8 – $Ce_3Ir_4Si_4$, τ_{10} – $Ce_6Ir_{30}Si_{19}$, τ_{12} – $Ce_2Ir_{12}Si_7$ and τ_{14} – $Ce_3Ir_3Si_2$ are fully ordered compounds with fixed compositions.

The quantitative data on the solubility of the ternary homogeneity regions at 950 °C are included in Table 1. The limits of solid solutions were established from the sets of EPMA measurements performed on the alloys containing the respective compound. Composition and lattice parameters of the phases involved in three-phase equilibria are listed in Table 2.

4.2. Crystal structure and composition of binary phases

X-ray powder diffraction intensities for unary and most of binary phases reported in literature agree well with those observed in ternary Ce-Ir-Si alloys of suitable compositions. However, the binaries $CeSi_{1.34}$, $IrSi_{3-x}$ and $CeIr_2$ require additional consideration.

$CeSi_{1.34}$ compound was detected by EPMA technique and found to participate in equilibria with CeSi and $CeSi_{2-x}$ (with 1 at.% of Ir) as shown in Fig. 1. SEM image of $Ce_{42.5}Ir_{0.5}Si_{57}$ (at.%) sample is shown in Fig. 2a and depicts all three phases in equilibria.

In our work, we did not detect reported in Ref. [43] wide homogeneity region of binary $CeIr_2$ phase from 30 to 37 at. % of Ce. EPMA measurements for all annealed at 950 °C ternary alloys from

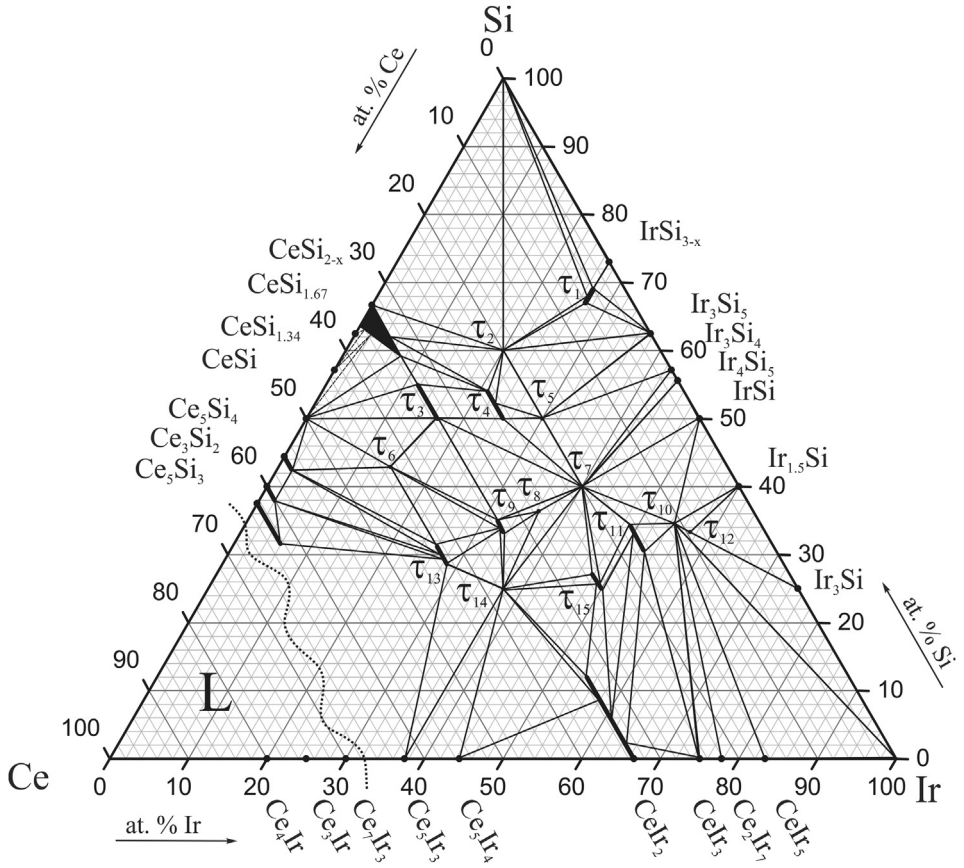

Fig. 1. Isothermal section of the Ce–Ir–Si system at 950 °C.

Table 2
Experimental data on alloys from three-phase regions in the Ce–Ir–Si system at 950 °C.

Three-phase field	Phase	EPMA (at.%)			Lattice parameters (nm)		
		Ce	Ir	Si	*a*	*b*	*c*
(Si) + $CeSi_{2-x}$ + τ_2	(Si)	0.0	0.0	100.0	0.54301(2)		
	$CeSi_{2-x}$	33.5	0.0	66.5	0.41911(1)		1.39706(6)
	τ_2	19.9	20.2	59.9	0.42440(2)		0.97912(4)
(Si) + τ_1 + τ_2	(Si)	0.0	0.0	100.0	0.54321(2)		
	τ_1	5.2	26.9	67.9	0.44369(3)		0.65840(6)
	τ_2	19.8	20.1	60.1	0.42433(2)		0.97916(4)
(Si) + $\alpha IrSi_{3-x}$ + τ_1	(Si)	0.0	0.0	100.0	0.54305(2)		
	$\alpha IrSi_{3-x}$	0.0	26.8	73.2	0.76888(4)	0.43714(3)	0.65401(3)
						$\beta = 91.59(2)^\circ$	
	τ_1	4.1	27.2	68.7	0.44329(7)		0.65788(7)
Ir_3Si_5 + τ_1 + τ_2	Ir_3Si_5	0.0	37.8	62.2	0.63994(4)	1.41455(9)	1.15515(7)
						$\beta = 116.65(1)^\circ$	
	τ_1	6.0	27.0	67.0	0.44394(8)		0.65948(9)
	τ_2	20.2	20.5	59.3	0.42449(3)		0.97923(5)
$\alpha IrSi_{3-x}$ + Ir_3Si_5 + τ_1	$\alpha IrSi_{3-x}$	0.0	27.3	72.7	0.76875(4)	0.43695(2)	0.65422(3)
						$\beta = 91.58(2)^\circ$	
	Ir_3Si_5	0.0	37.4	62.6	0.64011(3)	1.41423(9)	1.15480(8)
						$\beta = 116.66(2)^\circ$	
	τ_1	4.2	26.7	69.1	0.44322(4)		0.65778(4)
$CeSi_{2-x}$ + CeSi + τ_3	$CeSi_{2-x}$	33.4	7.1	59.5	0.41752(5)		1.4065(2)
	CeSi	50.2	0.0	49.8	0.82998(9)	0.39630(5)	0.59627(7)
	τ_3	33.4	11.6	55.0	0.8177(1)		0.42686(4)
$CeSi_{2-x}$ + τ_3 + τ_4	$CeSi_{2-x}$	33.3	8.0	58.7	0.41730(3)		1.40663(8)
	τ_3	33.1	11.9	55.0	0.81753(9)		0.42676(4)
	τ_4	24.5	21.0	54.5	0.42528(2)	1.6736(1)	0.41945(2)
$CeSi_{2-x}$ + τ_2 + τ_4	$CeSi_{2-x}$	33.6	5.5	60.9	0.41866(3)		1.3995(3)
	τ_2	20.1	20.0	59.9	0.42424(2)		0.97924(5)
	τ_4	24.8	21.1	54.1	0.42495(2)	1.6739(4)	0.41958(1)
τ_2 + τ_4 + τ_5	τ_2	20.0	19.9	60.1	0.42443(1)		0.97964(2)
	τ_4	25.2	22.8	52.0	0.42485(1)	1.6752(3)	0.41965(1)
	τ_5	20.2	30.0	49.8	0.99584(5)	1.15670(9)	0.58756(3)
Ir_3Si_5 + τ_2 + τ_5	Ir_3Si_5	0.0	37.5	62.5	0.64034(3)	1.4151(1)	1.15497(7)
						$\beta = 116.64(2)^\circ$	
	τ_2	20.1	20.4	59.5	0.42414(3)		0.97896(6)
	τ_5	20.1	29.7	50.2	0.99599(5)	1.15738(7)	0.58789(3)
Ir_3Si_5 + Ir_3Si_4 + τ_5	Ir_3Si_5	0.0	37.2	62.8	0.63981(3)	1.4144(4)	1.15456(6)
						$\beta = 116.65(2)^\circ$	
	Ir_3Si_4	0.0	43.1	56.9	1.8873(3)	0.36960(1)	0.57722(3)
	τ_5	19.7	29.9	50.4	0.99653(5)	1.15745(6)	0.58739(3)
Ce_5Si_3 + Ce_3Si_2 + τ_{13}	Ce_5Si_3	62.4	6.0	31.6	0.78727(7)		1.37935(9)
	Ce_3Si_2	59.9	1.9	38.2	0.77764(8)		0.43654(3)
	τ_{13}	42.9	27.6	29.5	0.41131(1)	1.08117(8)	1.33717(9)
Ce_3Si_2 + Ce_5Si_4 + τ_{13}	Ce_3Si_2	60.3	2.0	37.7	0.77774(7)		0.43649(2)
	Ce_5Si_4	55.3	2.1	42.6	0.79369(6)		1.5019(5)
	τ_{13}	43.4	26.6	30.0	0.41123(2)	1.08155(7)	1.33771(8)
Ce_5Si_4 + CeSi + τ_6	Ce_5Si_4	55.6	2.0	42.4	0.79394(5)		1.50213(9)
	CeSi	50.4	0.0	49.6	0.82926(4)	0.39627(1)	0.59590(3)
	τ_6	43.0	14.1	42.9	0.41123(2)	1.0815(2)	1.3381(2)
Ce_5Si_4 + τ_6 + τ_{13}	Ce_5Si_4	56.0	1.9	42.1	0.79382(4)		1.50233(9)
	τ_6	43.1	14.0	42.9	0.41327(2)	0.42759(2)	1.8184(4)
	τ_{13}	42.6	26.1	31.3	0.41113(1)	1.0821(1)	1.3380(2)
CeSi + τ_6 + τ_3	CeSi	49.8	0.0	50.2	0.82965(5)	0.39595(1)	0.59595(3)
	τ_6	42.5	14.3	43.2	0.41329(1)	0.42776(2)	1.8190(5)
	τ_3	33.3	16.8	49.9	0.82149(5)		0.42367(2)
τ_6 + τ_{13} + τ_9	τ_6	43.0	14.5	42.5	0.41307(1)	0.42740(1)	1.81796(9)
	τ_{13}	42.6	26.2	31.2	0.41123(4)	1.08200(7)	1.33804(9)
	τ_9	33.2	32.9	33.9	0.62733(1)		
τ_6 + τ_3 + τ_9	τ_6	42.4	15.1	42.5	0.41315(1)	0.42758(1)	1.81916(6)
	τ_3	33.1	17.1	49.8	0.82134(5)		0.42354(2)
	τ_9	33.3	31.5	35.2	0.62712(2)		
τ_3 + τ_9 + τ_7	τ_3	33.2	16.7	50.1	0.82159(4)		0.42359(2)
	τ_9	33.5	31.4	35.1	0.62709(4)		
	τ_7	20.3	40.0	39.7	0.41392(2)		0.98538(5)
τ_3 + τ_4 + τ_7	τ_3	33.5	16.5	50.0	0.82142(5)		0.42381(2)
	τ_4	24.8	25.3	49.9	0.42527(2)	1.67505(7)	0.41930(1)
	τ_7	19.8	40.4	39.8	0.41379(1)		0.98514(3)
τ_4 + τ_5 + τ_7	τ_4	25.0	25.0	50.0	0.42533(2)	1.6745(1)	0.41964(2)
	τ_5	20.5	29.7	49.8	0.99639(6)	1.15612(7)	0.58791(4)
	τ_7	20.4	39.8	39.8	0.41410(2)		0.98586(4)
Ir_3Si_4 + τ_5 + τ_7	Ir_3Si_4	0.0	42.6	57.4	1.88755(9)	0.36983(1)	0.57736(3)
	τ_5	20.6	29.9	49.5	0.99515(5)	1.15745(6)	0.58738(3)
	τ_7	20.5	39.8	39.7	0.41368(2)		0.98550(3)
IrSi + Ir_4Si_5 + τ_7	IrSi	0.0	50.2	49.8	0.55577(3)	0.32147(1)	0.62703(4)

Table 2 (*continued*)

Three-phase field	Phase	EPMA (at.%)			Lattice parameters (nm)		
		Ce	Ir	Si	*a*	*b*	*c*
	Ir_4Si_5	0.0	44.3	55.7	0.58814(3)	0.36193(1) β = 100.13(1)°	1.2352(1)
	τ_7	20.2	39.9	39.9	0.41393(1)		0.98542(3)
$Ce_5Ir_3 + \tau_{13} + \tau_{14}$	Ce_5Ir_3	62.5	37.5	0.0	1.12705(7)		0.63682(3)
	τ_{13}	42.5	28.9	28.6	0.41181(3)	1.08137(7)	1.33794(8)
	τ_{14}	37.1	37.8	25.1	0.76967(4)	1.48070(8)	0.57012(3)
$Ce_5Ir_3 + Ce_5Ir_4 + \tau_{14}$	Ce_5Ir_3	62.2	37.8	0.0	1.12711(5)		0.63685(2)
	Ce_5Ir_4	55.3	44.7	0.0	0.74372(5)	1.47803(9)	0.76261(5)
	τ_{14}	37.4	37.7	24.9	0.76926(5)	1.48069(9)	0.57048(3)
$\tau_{13} + \tau_9 + \tau_{14}$	τ_{13}	43.0	28.9	28.1	0.41196(2)	1.08141(5)	1.33809(7)
	τ_9	33.7	32.8	33.5	0.62757(5)		
	τ_{14}	37.5	38.4	24.1	0.76891(5)	1.4812(1)	0.57013(4)
$\tau_9 + \tau_8 + \tau_{14}$	τ_9	33.4	32.8	33.8	0.62761(3)		
	τ_8	27.8	36.2	36.0	0.40242(2)	0.41431(2)	2.4345(2)
	τ_{14}	37.7	37.6	24.7	0.76926(5)	1.4800(3)	0.57020(4)
$\tau_8 + \tau_7 + \tau_{14}$	τ_8	27.6	36.4	36.0	0.40218(1)	0.41448(2)	2.4339(1)
	τ_7	20.3	40.1	39.6	0.41406(2)		0.98553(4)
	τ_{14}	37.9	37.1	25.0	0.76904(5)	1.48146(10)	0.57079(4)
$\tau_7 + \tau_{14} + \tau_{15}$	τ_7	20.3	40.0	39.7	0.41374(1)		0.98591(3)
	τ_{14}	37.7	37.2	25.1	0.76977(4)	1.48127(7)	0.57009(3)
	τ_{15}	25.0	47.9	27.1	0.40665(2)		3.5322(2)
$CeIr_2 + \tau_{14} + \tau_{15}$	$CeIr_2$	33.7	54.3	12.0	0.75480(7)		
	τ_{14}	37.8	37.6	24.6	0.76885(5)	1.48051(8)	0.57087(4)
	τ_{15}	24.8	49.2	26.0	0.40674(1)		3.5314(5)
$Ce_5Ir_4 + CeIr_2 + \tau_{14}$	Ce_5Ir_4	55.7	44.3	0.0	0.74355(4)	1.47798(8)	0.76215(5)
	$CeIr_2$	33.5	58.0	8.5	0.75492(6)		
	τ_{14}	36.7	37.3	26.0	0.76897(5)	1.48137(9)	0.57018(3)
$\tau_7 + \tau_{15} + \tau_{11}$	τ_7	19.7	40.0	40.3	0.41387(1)		0.98538(3)
	τ_{15}	24.8	49.6	25.6	0.40626(1)		3.5388(8)
	τ_{11}	16.6	48.8	34.6	0.71783(5)	0.97301(8)	0.55978(4)
$\tau_7 + \tau_{11} + \tau_{10}$	τ_7	20.1	39.9	40.0	0.41369(2)		0.98491(5)
	τ_{11}	16.5	49.0	34.5	0.71769(5)	0.97312(7)	0.55974(5)
	τ_{10}	11.3	54.3	34.4	1.5706(2)		0.38863(1)
$IrSi + \tau_7 + \tau_{10}$	IrSi	0.0	50.1	49.9	0.55570(5)	0.32168(2)	0.62687(5)
	τ_7	20.2	39.7	40.1	0.41379(2)		0.98494(4)
	τ_{10}	11.0	54.9	34.1	1.5694(4)		0.38928(5)
$Ir_{1.5}Si + IrSi + \tau_{10}$	$Ir_{1.5}Si$	0.0	59.9	40.1	0.39620(1)		0.51235(3)
	IrSi	0.0	50.1	49.9	0.55569(3)	0.32150(1)	0.62731(3)
	τ_{10}	11.2	54.8	34.0	1.57094(7)		0.38954(6)
$CeIr_2 + \tau_{15} + \tau_{11}$	$CeIr_2$	33.5	60.6	5.9	0.75644(4)		
	τ_{15}	25.5	50.0	24.5	0.40603(4)		3.5397(3)
	τ_{11}	17.1	50.8	32.1	0.71801(4)	0.97271(5)	0.55928(4)
$CeIr_2 + CeIr_3 + \tau_{11}$	$CeIr_2$	32.5	64.8	2.7	0.75783(5)		
	τ_{11}	17.4	53.0	29.6	0.71819(5)	0.97263(8)	0.55932(4)
	$CeIr_3$	25.1	74.9	0.0	0.52920(2)		2.6199(8)
$CeIr_3 + \tau_{11} + \tau_{10}$	$CeIr_3$	25.0	75.0	0.0	0.52920(2)		2.6195(8)
	τ_{11}	17.1	53.1	29.8	0.71830(4)	0.97255(5)	0.55940(3)
	τ_{10}	11.2	54.1	34.7	1.5706(3)		0.38863(1)
$CeIr_3 + Ce_2Ir_7 + \tau_{10}$	$CeIr_3$	24.8	75.2	0.0	0.52943(2)		2.6195(9)
	Ce_2Ir_7	22.5	77.5	0.0	0.52943(6)		3.9011(8)
	τ_{10}	10.9	54.3	34.8	1.5714(2)		0.38929(5)
$Ir_3Si + Ir_{1.5}Si + \tau_{12}$	Ir_3Si	0.0	74.8	25.2	0.52220(4)		0.79631(6)
	$Ir_{1.5}Si$	0.0	60.1	39.9	0.39649(2)		0.51229(3)
	τ_{12}	9.5	56.8	33.7	0.97366(6)		0.38641(2)
$(Ir) + CeIr_5 + \tau_{10}$	(Ir)	0.0	100.0	0.0	0.38394(3)		
	$CeIr_5$	16.2	83.8	0.0	0.5298(2)		0.4260(1)
	τ_{10}	11.0	54.5	34.5	1.5713(2)		0.38924(1)
$(Ir) + Ir_3Si + \tau_{10}$	(Ir)	0.0	100.0	0.0	0.38410(1)		
	Ir_3Si	0.0	75.0	25.0	0.52235(5)		0.79601(8)
	τ_{10}	11.0	55.1	33.9	1.5708(2)		0.38902(1)

both Ce-rich and Ir-rich sides of $CeIr_2$ as well as $Ce_{50}Ir_{50}$ (at.%) sample (Fig. 2b) revealed the cerium content about 33 at.%.

In order to check literature data about binary $IrSi_{3-x}$ with unknown crystal structure we prepared and investigated $Ir_{25}Si_{75}$ (at.%) alloy. The SEM study of annealed sample revealed a microstructure composed of small inclusions of pure silicon crystallites (Fig. 2c) and the main matrix of $IrSi_{3-x}$ phase with $Ir_{26.5}Si_{73.5}$ (at.%) composition, which is in line with reported by Engström et al. [54] ($Ir_{26}Si_{74}$, at.%). Regions with slightly different darkness in the main matrix but with identical composition could be attributed to different crystallographic orientation of $IrSi_{3-x}$ crystallites (Fig. 2c). Since the phase transition between high and low temperature modifications of $IrSi_{3-x}$ occurs at 975 °C, in our work we observed the crystal structures of both phases in XPD patterns (see Fig. 3). After annealing of the $Ir_{25}Si_{75}$ (at.%) sample, a high temperature orthorhombic β$IrSi_{3-x}$ phase undergoes unit cell distortion and becomes a monoclinic α$IrSi_{3-x}$ with similar cell parameters and β = 91.60° (see Table 1). The full information about the atomic orders in the α and β modifications of $IrSi_{3-x}$ was not obtained.

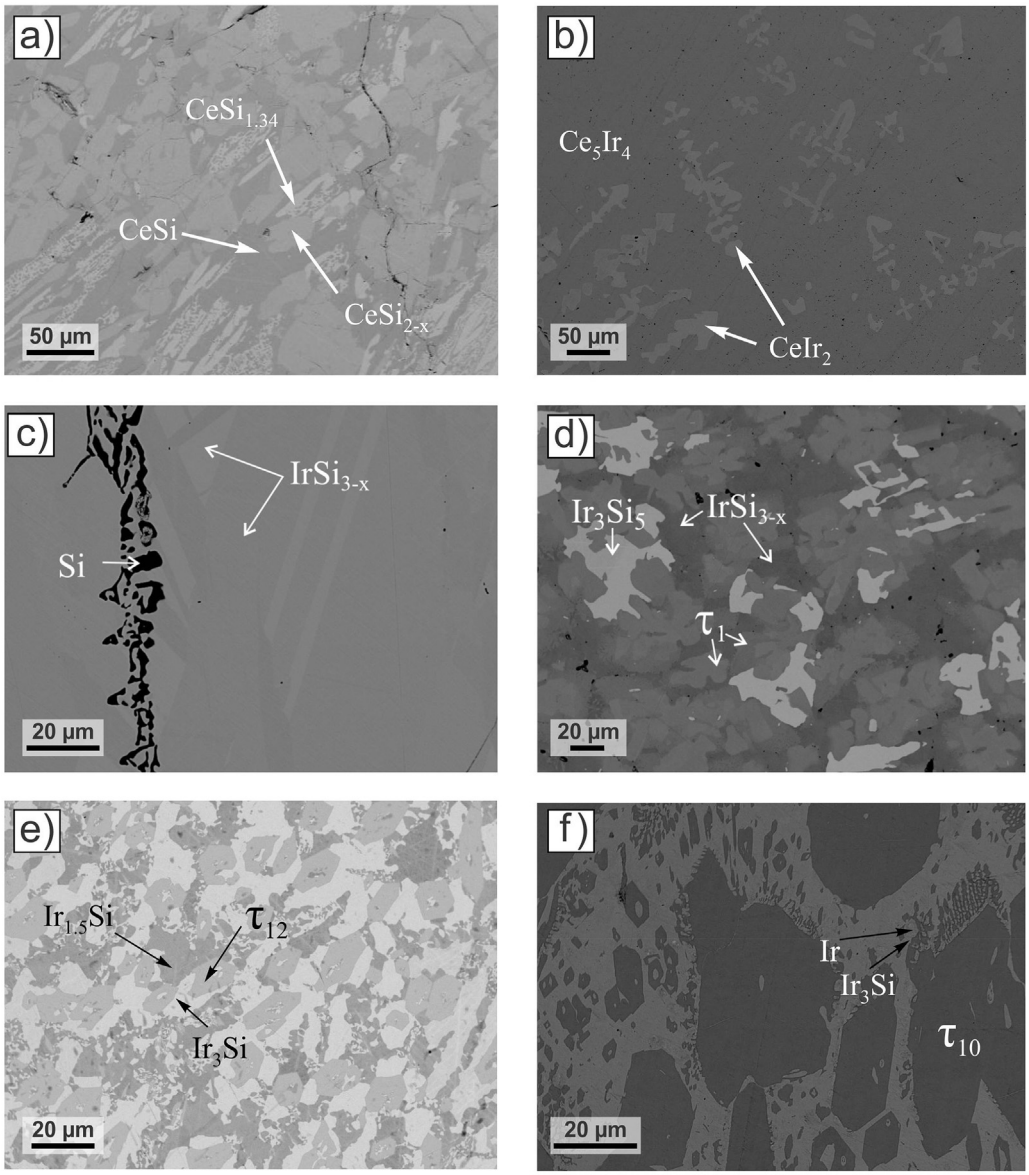

Fig. 2. Microstructures (SEM) of $Ce_{42.5}Ir_{0.5}Si_{57}$ (at.%, *a*), $Ce_{50}Ir_{50}$ (at.%, *b*), $Ir_{25}Si_{75}$ (at.%, *c*), $Ce_3Ir_{28}Si_{69}$ (at.%, *d*), $Ce_2Ir_{66}Si_{32}$ (at.%, *e*), and $Ce_7Ir_{63}Si_{30}$ (at.%, *f*) alloys annealed at 950 °C.

4.3. Crystal structure and composition of ternary phases

The atomic orders of all previously reported in literature ternary intermetallics were confirmed in the present investigation. Eight ternary compounds of the Ce–Ir–Si system were previously found and their structure described prior to this work: $CeIrSi_3$ ($BaNiSn_3$-type) [17,18], $CeIrSi_2$ ($CeNiSi_2$-type) [19], $Ce_2Ir_3Si_5$ ($U_2Co_3Si_5$-type) [20], CeIrSi (LaIrSi-type) [21], $CeIr_2Si_2$ (α and β forms, $ThCr_2Si_2$-type and $CaBe_2Ge_2$-type, correspondingly [22,23]), $CeIr_{2-x}Si_{1+x}$ ($CeIr_2Si$-type) [24], Ce_2IrSi_3 (Ce_2CoSi_3-type) [25], and $CeIr_3Si_2$ ($ErRh_3Si_2$-type) [26,27].

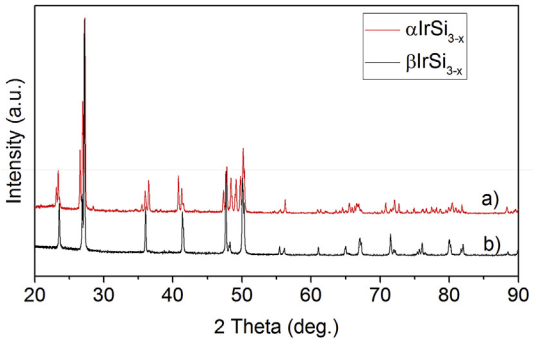

Fig. 3. X-ray powder patterns of the as-cast (a) and annealed (b) $Ir_{25}Si_{75}$ (at.%) alloys.

Based on X-ray powder diffraction data the crystal structures for six new ternary phases were assigned to known structure types: τ_6 – Ce_3IrSi_3 (Ta_3B_4-type), τ_8 – $Ce_3Ir_4Si_4$ ($U_3Ni_4Si_4$-type), τ_{10} – $Ce_6Ir_{30}Si_{19}$ ($Sc_6Co_{30}Si_{19}$-type), τ_{12} – $Ce_2Ir_{12}Si_7$ ($Ho_2Rh_{12}As_7$-type), τ_{13} – $Ce_3Ir_{2-x}Si_{2+x}$ ($Sm_3Ir_2Si_2$-type), and τ_{14} – $Ce_3Ir_3Si_2$ ($Ce_3Rh_3Si_2$-type). Crystal structure types, space groups and lattice parameters of ternary intermetallics found in the Ce-Ir-Si system at 950 °C are collected in Table 1.

τ_1 – $Ce_4Ir_{27}Si_{69}$ is a new ternary compound detected by EPMA in the Si-rich corner of the Ce-Ir-Si system. It participates in equilibria with Si, $CeIrSi_3$, Ir_3Si_5 and $IrSi_{3-x}$, exhibiting homogeneity region

Table 3
Experimental details and crystallographic data for $\tau_3 - Ce_2IrSi_3$, $\tau_6 - Ce_3IrSi_3$, $\tau_8 - Ce_3Ir_4Si_4$, $\tau_{10} - Ce_6Ir_{30}Si_{19}$, $\tau_{12} - Ce_2Ir_{12}Si_7$, $\tau_{13} - Ce_3Ir_2Si_2$, $\tau_{14} - Ce_3Ir_3Si_2$, derived from the powder X-ray diffraction intensities (room temperature, CuKα_1 radiation).

Compound	**$\tau_6 - Ce_3IrSi_3$**	**$\tau_8 - Ce_3Ir_4Si_4$**	**$\tau_{10} - Ce_6Ir_{30}Si_{19}$**
Space group	*Immm* (No 71)	*Immm* (No 71)	$P6_3/m$ (No 176)
Pearson symbol	*oI*14	*oI*22	*hP*55
Structure type	Ta_3B_4	$U_3Ni_4Si_4$	$Sc_6Co_{30}Si_{19}$
Lattice parameters, [nm]	$a = 0.41323(1)$	$a = 0.40241(2)$	$a = 1.57154(3)$
	$b = 0.42755(1)$	$b = 0.41430(2)$	
	$c = 1.8182(1)$	$c = 2.4345(1)$	$c = 0.38915(1)$
Cell volume, [nm^3]	0.32132(2)	0.40588(3)	0.83233(1)
2θ range, [°]	$8 \le 2\theta \le 90$	$10 \le 2\theta \le 90$	$8 \le 2\theta \le 90$
Number of reflections	110	135	307
Number of parameters	21	20	36
$R_F = \Sigma\lvert F_o\text{-}F_c\rvert/\Sigma F_o$	0.038	0.080	0.037
$R_I = \Sigma\lvert I_o\text{-}I_c\rvert/\Sigma I_o$	0.040	0.143	0.045
$R_{wP} = [\Sigma w_i\lvert y_{oi}\text{-}y_{ci}\rvert^2/\Sigma w_i\lvert y_{oi}\rvert^2]^{½}$	0.035	0.103	0.065
$R_P = \Sigma\lvert y_{oi}\text{-}y_{ci}\rvert/\Sigma\lvert y_{0i}\rvert$	0.027	0.078	0.047
$R_e = [(N\text{-}P + C)/\Sigma w_i y^2_{oi})]^{½}$	0.018	0.041	0.011
$\chi^2 = (R_{wP}/R_e)^2$	1.64	6.24	1.85
Atomic parameters			
Atom site 1	**2 Ce1** in 2*a* (0,0,0);	**2 Ce1** in 2*a* (0,0,0);	**6 Ce1** in 6*h* (*x*,*y*,¼);
			$x = 0.2966(3)$,
			$y = 0.3984(2)$
Occupation	1.0(−)	1.0(−)	1.0(−)
B_{iso} (10^2 nm^2)	1.9(1)	1.09(9)	0.98(4)
Atom site 2	**4 Ce2** in 4*j* (½,0,*z*);	**4 Ce2** in 4*j* (½,0,*z*);	**6 Ir1** in 6*h* (*x*,*y*,¼);
	$z = 0.1840(1)$	$z = 0.3553(2)$	$x = 0.0477(2)$,
			$y = 0.2755(2)$
Occupation	1.0(−)	1.0(−)	1.0(−)
B_{iso} (10^2 nm^2)	1.2(1)	1.09(9)	0.72(1)
Atom site 3	**4 M** in 4*i* (0,0,*z*);	**4 Ir1** in 4*i* (0,0,*z*);	**6 Ir2** in 6*h* (*x*,*y*,¼);
	$z = 0.4331(1)$	$z = 0.2490(1)$	$x = 0.1233(2)$,
			$y = 0.1520(1)$
Occupation	0.51(1) Si + 0.49(1) Ir	1.0(−)	1.0(−)
B_{iso} (10^2 nm^2)	1.3(1)	0.84(6)	0.72(1)
Atom site 4	**4 Si1** in 4*j* (½,0,*z*);	**4 Ir2** in 4*j* (½,0,*z*);	**6 Ir3** in 6*h* (*x*,*y*,¼);
	$z = 0.3641(4)$	$z = 0.0980(1)$	$x = 0.2230(1)$,
			$y = 0.5704(2)$
Occupation	1.0(−)	1.0(−)	1.0(−)
B_{iso} (10^2 nm^2)	1.1(1)	0.84(6)	0.72(1)
Atom site 5		**4 Si1** in 4*i* (0,0,*z*);	**6 Ir4** in 6*h* (*x*,*y*,¼);
		$z = 0.4590(8)$	$x = 0.4168(2)$,
			$y = 0.2622(2)$
Occupation		1.0(−)	1.0(−)
B_{iso} (10^2 nm^2)		1.5(3)	0.72(1)
Atom site 6		**4 Si2** in 4*j* (½,0,*z*);	**6 Ir5** in 6*h* (*x*,*y*,¼);
		$z = 0.1899(8)$	$x = 0.5359(2)$,
			$y = 0.0760(2)$
Occupation		1.0(−)	1.0(−)
B_{iso} (10^2 nm^2)		1.5(3)	0.72(1)
Atom site 7			**6 Si1** in 6*h* (*x*,*y*,¼);
			$x = 0.0678(9)$,
			$y = 0.4335(9)$
Occupation			1.0(−)
B_{iso} (10^2 nm^2)			0.46(8)
Atom site 8			**6 Si2** in 6*h* (*x*,*y*,¼);
			$x = 0.2486(8)$,
			$y = 0.1260(10)$
Occupation			1.0(−)
B_{iso} (10^2 nm^2)			0.46(8)
Atom site 9			**6 Si3** in 6*h* (*x*,*y*,¼);
			$x = 0.5608(8)$,
			$y = 0.2390(9)$
Occupation			1.0(−)
B_{iso} (10^2 nm^2)			0.46(8)
Atom site 9			**1 Si4** in 2*a* (0,0,¼);
Occupation			0.47(6)
B_{iso} (10^2 nm^2)			0.46(8)

Compound	**$\tau_{12} - Ce_2Ir_{12}Si_7$**	**$\tau_{13} - Ce_3Ir_2Si_2$**	**$\tau_{14} - Ce_3Ir_3Si_2$**
Space group	$P6_3/m$ (No 176)	*Cmcm* (No 63)	*Pnma* (No 62)
Pearson symbol	*hP*21	*oC*28	*oP*32
Structure type	$Ho_2Rh_{12}As_7$	$Sm_3Ir_2Si_2$	$Ce_3Rh_3Si_2$
Lattice parameters, [nm]	$a = 0.97330(4)$	$a = 0.41178(2)$	$a = 0.76950(2)$
		$b = 1.08136(4)$	$b = 1.48111(4)$

(*continued on next page*)

Table 3 (*continued*)

Compound	**τ_{12} – $Ce_2Ir_{12}Si_7$**	**τ_{13} – $Ce_3Ir_2Si_2$**	**τ_{14} – $Ce_3Ir_3Si_2$**
	c = 0.38664(2)	c = 1.33775(6)	c = 0.57065(2)
Cell volume, [nm^3]	0.31722(3)	0.59567(4)	0.65038(3)
2θ range, [°]	10 ≤ 2θ ≤ 90	10 ≤ 2θ ≤ 90	10 ≤ 2θ ≤ 90
Number of reflections	117	170	309
Number of parameters	17	16	26
$R_F = \Sigma\|F_o\text{-}F_c\|/\Sigma F_o$	0.036	0.046	0.048
$R_I = \Sigma\|I_o\text{-}I_c\|/\Sigma I_o$	0.055	0.082	0.080
$R_{wP} = [\Sigma w_i\|y_{oi}\text{-}y_{ci}\|^2/\Sigma w_i\|y_{oi}\|^2]^{½}$	0.146	0.076	0.116
$R_P = \Sigma\|y_{oi}\text{-}y_{ci}\|/\Sigma\|y_{oi}\|$	0.112	0.058	0.091
$R_e = [(N\text{-}P + C)/\Sigma w_i y^2_{oi})]^{½}$	0.105	0.044	0.093
$\chi^2 = (R_{wP}/R_e)^2$	1.90	3.04	1.57
Atomic parameters			
Atom site 1	**2 Ce1** in 2*d* (2/3,1/3,1/4);	**8 Ce1** in 8*f* (0,*y*,*z*); *y* = 0.2287(3), *z* = 0.1018(2)	**8 Ce1** in 8*d* (*x*,*y*,*z*); *x* = 0.0228(3), *y* = 0.1109(2), *z* = 0.6391(5)
Occupation	1.0(−)	1.0(−)	1.0(−)
B_{iso} (10^2 nm^2)	1.9(4)	0.54(7)	0.74(7)
Atom site 2	**6 Ir1** in 6*h* (*x*,*y*,¼); *x* = 0.0626(9), *y* = 0.4475(11)	**4 Ce2** in 4*c* (0,*y*,¼); *y* = 0.5239(4)	**4 Ce2** in 4*c* (*x*,¼,*z*); *x* = 0.1675(7), *z* = 0.0974(9)
Occupation	1.0(−)	1.0(−)	1.0(−)
B_{iso} (10^2 nm^2)	0.89(10)	0.54(7)	0.74(7)
Atom site 3	**6 Ir2** in 6*h* (*x*,*y*,¼); *x* = 0.2628(6), *y* = 0.1426(10)	**4 Ir1** in 4*c* (0,*y*,¼); *y* = 0.8146(3)	**8 Ir1** in 8*d* (*x*,*y*,*z*); *x* = 0.1652(4), *y* = 0.0400(1), *z* = 0.1057(5)
Occupation	1.0(−)	1.0(−)	1.0(−)
B_{iso} (10^2 nm^2)	0.89(10)	0.88(7)	0.94(5)
Atom site 4	**6 Si1** in 6*h* (*x*,*y*,¼); *x* = 0.289(6), *y* = 0.413(5)	**4 Ir2** in 4*b* (0,½,0);	**4 Ir2** in 4*c* (*x*,¼,*z*); *x* = 0.3188(6), *z* = 0.5625(6)
Occupation	1.0(−)	1.0(−)	1.0(−)
B_{iso} (10^2 nm^2)	2.8(8)	0.88(7)	0.94(5)
Atom site 5	**1 Si1** in 4*e* (0,0,*z*); *z* = 0.092(1)	**8 Si1** in 8*f* (0,*y*,*z*); *y* = 0.946(2), *z* = 0.093(1)	**8 Si1** in 8*d* (*x*,*y*,*z*); *x* = 0.358(2), *y* = 0.1146(9), *z* = 0.428(2)
Occupation	0.25(1)	1.0(−)	1.0(−)
B_{iso} (10^2 nm^2)	2.8(8)	1.5(3)	1.6(3)

from $Ce_4Ir_{27}Si_{69}$ to $Ce_6Ir_{27}Si_{67}$ at. %. This unique homogeneity region along iso-concentration line of 27 at. % Ir assumes the unusual substitution of small silicon atoms by significantly larger cerium ones. Also, the iridium concentration is identical to non-stoichiometric $IrSi_{3-x}$ phase, but there is a clear boundary between these two phases as seen in SEM images of $Ce_3Ir_{28}Si_{69}$ (at.%) alloy (see Fig. 2d). This indicates that these two compounds are related but are essentially different phases. The XPD study of $Ce_3Ir_{28}Si_{69}$ alloy demonstrates the presence of monoclinic phases Ir_3Si_5 and αIrSi$_{3-x}$ together with a new phase which was indexed in hexagonal symmetry with parameters a = 0.44329 nm and b = 0.65788 nm. These parameters of τ_1 phase, converted to orthorhombic ($a' = a\sqrt{3}$; a' = 0.7685 nm, b = 0.4437 nm, c = 0.6586 nm), are similar to the cell parameters of βIrSi$_{3-x}$. Further studies of unconventional homogeneity region of τ_1 phase and its complete structural information of the atomic order are needed.

τ_6 – *Ce_3IrSi_3* crystallizes with the orthorhombic structure of the Ta_3B_4-type, space group *Immm*, lattice parameters a = 0.41323(1) nm, b = 0.42755(1) nm, and c = 1.8182(1) nm. Preliminary SEM and EPMA tests of the alloy with exact 3:1:3 stoichiometry indicated single phase state of the prepared sample. The set of the experimental peaks of a XPD pattern was successfully indexed in orthorhombic unit cell with the dimensions ~0.41 × 0.43 × 1.81 nm, similar to those for the related compound Ce_3RhSi_3, which had been studied before [9]. Further Rietveld refinement of the XPD pattern revealed the crystal structure to be isotypic with Ce_3RhSi_3 (Ta_3B_4 type of the crystal structure, see Table 3).

τ_8 – *$Ce_3Ir_4Si_4$*. The phase of 3:4:4 stoichiometry composition (~$Ce_{27}Ir_{36.5}Si_{36.5}$ at.%) was not detected by EPMA and SEM techniques in as-cast alloys. However, the new phase was observed in the annealed samples in equilibrium with known compounds CeIrSi and $CeIr_2Si_2$. $U_3Ni_4Si_4$-type as a model of the atomic order was successfully utilized in the Rietveld refinement. Space group *Immm* (No. 71), unit cell parameters a = 0.40241(2) nm, b = 0.41430(2) nm, c = 2.4345(1) nm. A set of experimental conditions and results of refinement are presented in Table 3.

τ_{10} – $Ce_6Ir_{30}Si_{19}$ and τ_{12} – $Ce_2Ir_{12}Si_7$. Two hexagonal ternary compounds, τ_{10} – $Ce_6Ir_{30}Si_{19}$ ($Sc_6Co_{30}Si_{19}$-type) and τ_{12} – $Ce_2Ir_{12}Si_7$ ($Ho_2Rh_{12}As_7$-type), were found in the high iridium content area of the Ce–Ir–Si phase diagram. These two compounds belong to a hexagonal structure series with linked triangular columns following the general formula $Ce_{n(n+1)}T_{6(n^2+1)}Si_{4n^2+3}$ and described in Refs. [9,60,61] (n = 1 for τ_{12} – $Ce_2Ir_{12}Si_7$, n = 2 for τ_{10} – $Ce_6Ir_{30}Si_{19}$). In contrast to analogous ternary Ce-Rh-Si system [9], other members of this series with $n = \infty$, 3 and 4 were not observed in Ce–Ir–Si system at 950 °C. Fig. 2e and f shows SEM images of $Ce_2Ir_{66}Si_{32}$ and $Ce_7Ir_{63}Si_{30}$ (at.%) alloys revealing two ternary equilibria: $Ir_{1.5}Si$ – Ir_3Si – τ_{12} and Ir – Ir_3Si – τ_{10}. Since τ_{12} is located exactly between τ_{10} and Ir_3Si phases (i.e. pure τ_{12} can be obtained by mixing τ_{10} and Ir_3Si), there is a degenerate triangle near τ_{12} – $Ce_2Ir_{12}Si_7$ phase (see Fig. 1). The results of the Rietveld refinements

of τ_{10} and τ_{12} phases are presented in Table 3.

τ_{13} – $Ce_3Ir_{2-x}Si_{2+x}$. Powder XPD pattern of $Ce_3Ir_2Si_2$ revealed orthorhombic symmetry of the new compound, the crystal structure of which was found to be isotopic to ternary $Sm_3Ir_2Si_2$, a site occupancy variant of the W_3CoB_3 type structure [62]. Rietveld analysis presented in Table 3 confirmed that $Ce_3Ir_2Si_2$ belongs to $Sm_3Ir_2Si_2$ crystal type with the space group *Cmcm* (No. 63), *oC*28, cell parameters $a = 0.41178(2)$ nm, $b = 1.08136(4)$ nm, $c = 1.33775(6)$ nm, $V = 0.59567(4)$ nm^3 and $Z = 4$ formula units per cell. The Ir–Si distances range from 0.246 to 0.254 nm, which is an indication of strong bonding [62]. $Ce_3Ir_{2-x}Si_{2+x}$ exhibits a homogeneity region along 42.9 at.% of Ce iso-concentrate line with Si concentration ranging from 28.5 to 31.5 at.% (i.e., $0.0 < x < 0.2$), see Fig. 1 and Table 1.

τ_{14} – $Ce_3Ir_3Si_2$. The compound with the same stoichiometry is observed in Ce-Rh-Si ternary system [4], and XPD pattern of $Ce_3Ir_3Si_2$ revealed similarities with $Ce_3Rh_3Si_2$ pattern. The results of Rietveld analysis presented in Table 3 confirmed that $Ce_3Ir_3Si_2$ belongs to $Ce_3Rh_3Si_2$ structural type with space group *Pnma* (No. 62), *oP*32, cell parameters $a = 0.76950(2)$ nm, $b = 1.48111(4)$ nm, $c = 0.57065(2)$ nm, $V = 0.65038(3)$ nm^3 and $Z = 4$ formula units per cell. The structure can be presented as an intergrowth of FeB- and YPd_2Si-type slabs [63]. At 950 °C $Ce_3Ir_3Si_2$ participates in equilibria with 5 ternary and three binary Ce–Ir phases, and has no homogeneity region.

5. Summary

Phase relations in the ternary system Ce–Ir–Si at 950 °C have been established based on 83 alloys, which were characterized by XPD, SEM and EMPA techniques. Fifteen ternary compounds were detected. Among them 8 phases have been reported earlier and their crystal structures were confirmed in the present work. Structure prototypes are assigned to six new Ce–Ir–Si compounds and the crystal structure of one new ternary intermetallic τ_1–$Ce_4Ir_{27}Si_{69}$ (at.%) is unknown. Except for the τ_1 compound, which exhibit homogeneity region along Ir iso-concentrate, binary and ternary iridium silicides do not dissolve cerium. Mutual solubility between silicon and iridium, however, results in formation of extended homogeneity regions for many compounds in the Ce–Ir–Si system.

Acknowledgements

This study was supported by the Russian Foundation for Basic Researches (Grant No 15-03-06767a). X-ray and EPMA measurements were performed at User Facilities Center of Lomonosov Moscow State University under support of Ministry of Education and Science of Russia, Contract N16.552.11.7081.

References

[1] P. Misra, Heavy-fermion Systems, Elsevier, 2008.
[2] N.D. Mathur, F.M. Grosche, S.R. Julian, I.R. Walker, D.M. Freye, R.K.W. Haselwimmer, G.G. Lonzarich, Magnetically mediated superconductivity in heavy fermion compounds, Nature 394 (1998) 39–43.
[3] H.R. Ott, Ch Wälti, Trends in superconductivity of heavy-electron metals, J. Supercond. Inc. Nov. Magn. 13 (2000) 837–846.
[4] G.R. Stewart, Non-Fermi-liquid behavior in d- and f-electron metals, Rev. Mod. Phys. 73 (2001) 797–855.
[5] F. Steglich, Superconductivity, magnetic ordering and non-Fermi-liquid effects in heavy-fermion metals, J. Magn. Magn. Mater. 226–230 (2001) 1–4.
[6] F. Kneidinger, E. Bauer, I. Zeiringer, P. Rogl, C. Blaas-Schenner, D. Reith, R. Podloucky, Superconductivity in non-centrosymmetric materials, Phys. C Supercond. Appl. 514 (2015) S388–S398.
[7] A. Gribanov, A. Grytsiv, E. Royanian, P. Rogl, E. Bauer, G. Giester, Y. Seropegin, On the system cerium–platinum–silicon, J. Solid State Chem. 181 (2008) 2964–2975.
[8] A. Lipatov, A. Gribanov, A. Grytsiv, P. Rogl, E. Murashova, Y. Seropegin, G. Giester, K. Kalmykov, The ternary system cerium–palladium–silicon, J. Solid State Chem. 182 (2009) 2497–2509.
[9] A. Lipatov, A. Gribanov, A. Grytsiv, S. Safronov, P. Rogl, J. Rousnyak, Y. Seropegin, G. Giester, The ternary system cerium–rhodium–silicon, J. Solid State Chem. 183 (2010) 829–843.
[10] F. Steglich, J. Aarts, C.D. Bredl, W. Lieke, D. Meschede, W. Franz, H. Schäfer, Superconductivity in the presence of strong Pauli paramagnetism: $CeCu_2Si_2$, Phys. Rev. Lett. 43 (1979) 1892–1896.
[11] W. Bażela, The influence of the crystal structure on the magnetic ordering in RT_2X_2 and RTX_3 compounds, J. Alloys Compd. 442 (2007) 132–135.
[12] C. Petrovic, P.G. Pagliuso, M.F. Hundley, R. Movshovich, J.L. Sarrao, M. Jaime, J.D. Thompson, Z. Fisk, P. Monthoux, Heavy-fermion superconductivity in $CeCoIn_5$ at 2.3 K, J. Phys. Condens. Matter 13 (2001) L337–L342.
[13] P.G. Pagliuso, J.D. Thompson, M.F. Hundley, J.L. Sarrao, Z. Fisk, Crystal structure and low-temperature magnetic properties of R_mMIn_{3m+2} compounds (M=Rh or Ir; m=1,2; R=Sm or Gd), Phys. Rev. B 63 (2001) 054426.
[14] J.I. Facio, D. Betancourth, P. Pedrazzini, V.F. Correa, V. Vildosola, D.J. García, P.S. Cornaglia, Why the Co-based 115 compounds are different: the case study of $GdMIn_5$ (M = Co,Rh,Ir), Phys. Rev. B 91 (2015) 014409.
[15] E. Bauer, G. Hilscher, H. Michor, Ch Paul, E.W. Scheidt, A. Gribanov, Yu Seropegin, H. Noël, M. Sigrist, P. Rogl, Heavy fermion superconductivity and magnetic order in noncentrosymmetric $CePt_3Si$, Phys. Rev. Let. 92 (2004) 027003.
[16] A. Gribanov, A. Grytsiv, P. Rogl, Y. Seropegin, G. Giester, Crystal structures of $RPt_{3-x}Si_{1-y}$ (R = Y, Tb, Dy, Ho, Er, Tm, Yb) studied by single crystal X-ray diffraction, J. Solid State Chem. 182 (2009) 1921–1928.
[17] P. Haen, P. Lejay, B. Chevalier, B. Lloret, J. Etourneau, M. Sera, Low-temperature magnetic and electrical properties of the new ternary silicides $LaMSi_3$ and $CeMSi_3$ with M ≡ Co, Rh, Ir, Ru, Os, J. Less-Common Met. 110 (1985) 321–325.
[18] Y. Muro, D. Eom, N. Takeda, M. Ishikawa, Contrasting Kondo-lattice behavior in $CeTSi_3$ and $CeTGe_3$ (T = Rh and Ir), J. Phys. Soc. Jpn. 67 (1998) 3601–3604.
[19] B. Chevalier, P. Rogl, K. Hiebl, J. Etourneau, On the intermediate valence of ternary silicides $CeRhSi_2$ and $CeIrSi_2$, J. Solid State Chem. 107 (1993) 327–331.
[20] C. Godart, C.V. Tomy, L.C. Gupta, R. Vijayaraghavan, Moment instabilities and magnetic ordering in $Ce_2Rh_3Ge_5$ and $Ce_2Ir_3Ge_5$, Solid State Commun. 67 (1988) 677–680.
[21] B. Heying, R. Pöttgen, M. Valldor, U.C. Rodewald, R. Mishra, R.D. Hoffmann, Synthesis, structure, and magnetic properties of the silicides REIrSi (RE = Ce, Pr, Er, Tm, Lu) and $SmIr_{0.266(8)}Si_{1.734(8)}$, Monatsh. Chem. 135 (2004) 1335–1347.
[22] K. Hiebl, C. Horvath, P. Rogl, Magnetic behavior of ternary silicides CeT_2Si_2, (T = Ru, Rh, Pd, OS, Ir, Pt) and boron substitution in $Ce\{Ru,Os\}_2Si_{2-x}B_x$, J. Less-Common Met. 117 (1986) 375–383.
[23] D. Niepmann, R. Pöttgen, A single crystal study of α-$CeIr_2Si_2$, β-$CeIr_2Si_2$ and $CeIr_{1.968(5)}Ge_2$, Intermetallics 9 (2001) 313–318.
[24] A. Gribanov, A. Grytsiv, P. Rogl, Y. Seropegin, G. Giester, X-ray structural study of intermetallic alloys RT_2Si and $RTSi_2$ (R = rare earth, T = noble metal), J. Solid State Chem. 183 (2010) 1278–1289.
[25] M. Szlawska, D. Kaczorowski, Antiferromagnetic order and Kondo effect in single-crystalline Ce_2IrSi_3, Phys. Rev. B 84 (2011) 094430 (1-6).
[26] Y. Muro, Y. Ohno, T. Okada, K. Motoya, Multi-step metamagnetism in $CeIr_3Si_2$, J. Magn. Magn. Mater. 310 (2007) 389–390.
[27] K. Motoya, Y. Muro, T. Takabatake, Real-time observation of magnetic structural change in the multistep metamagnet $CeIr_3Si_2$, J. Phys. Conf. Ser. 251 (2010) 012019 (1-4).
[28] I. Sugitani, Y. Okuda, H. Shishido, T. Yamada, A. Thamizhavel, E. Yamamoto, T.D. Matsuda, Y. Haga, T. Takeuchi, R. Settai, Y. Onuki, Pressure-induced heavy-fermion superconductivity in antiferromagnet $CeIrSi_3$ without inversion symmetry, J. Phys. Soc. Jpn. 75 (2006) 043703 (1-4).
[29] Y. Okuda, Y. Miyauchi, Y. Ida, Y. Takeda, C. Tonohiro, Y. Oduchi, T. Yamada, N.D. Dung, T.D. Matsuda, Y. Haga, T. Takeuchi, M. Hagiwara, K. Kindo, H. Harima, K. Sugiyama, R. Settai, Y. Onuki, Magnetic and superconducting properties of $LaIrSi_3$ and $CeIrSi_3$ with the non-centrosymmetric crystal structure, J. Phys. Soc. Jpn. 76 (2007) 044708 (1-11).
[30] N. Tateiwa, Y. Haga, T.D. Matsuda, S. Ikeda, E. Yamamoto, Y. Okuda, Y. Miyauchi, R. Settai, Y. Onuki, Strong-coupling superconductivity of $CeIrSi_3$ with the non-centrosymmetric crystal structure, J. Phys. Soc. Jpn. 76 (2007) 083706 (1-4).
[31] R. Settai, Y. Miyauchi, T. Takeuchi, F. Lévy, I. Sheikin, Y. Onuki, Huge upper critical field and electronic instability in pressure-induced superconductor $CeIrSi_3$ without inversion symmetry in the crystal structure, J. Phys. Soc. Jpn. 77 (2008) 073705 (1-4).
[32] D.T. Adroja, B.D. Rainford, Antiferromagnetic Kondo lattice: $CePdSi_2$, Phys. B 230–232 (1997) 762–765.
[33] M. Mihalik, M. Divis, V. Sechovský, Electronic and crystal structure of α- and β-$CeIr_2Si_2$, Phys. B 404 (2009) 3191–3194.
[34] C. Godart, L.C. Gupta, C.V. Tomy, S. Patil, R. Nagarajan, E. Beaurepaire, R. Vijayaraghavan, J.V. Yakhmi, Magnetism and mixed valence in some $R_2M_3X_5$ compounds: R = Ce, Eu, U; M = d metals, X = Si, Ge, Mat. Res. Bull. 23 (1988) 1781–1785.
[35] C. Godart, L.C. Gupta, C.V. Tomy, S. Patil, R. Nagarajan, E. Beaurepaire, R. Vijayaraghavan, Magnetism and mixed valence in some $R_2M_3X_5$ compounds: R = Ce, Eu; M = d metals, X = Si, Ge, Phys. B 163 (1990) 163–166.
[36] M. Szlawska, D. Kaczorowski, Antiferromagnetic ordering in single-crystalline Ce_2IrSi_3, J. Korean Phys. Soc. 62 (2013) 1564–1566.

[37] K. Motoya, Y. Muro, T. Takabatake, Long-time variation of magnetic structure in $CeIr_3Si_2$, J. Phys. Conf. Ser. 200 (2010) 032048 (1-4).
[38] K. Shigetoh, A. Ishida, Y. Ayabe, T. Onimaru, K. Umeo, Y. Muro, K. Motoya, M. Sera, T. Takabatake, Easy-plane magnetocrystalline anisotropy in the multistep metamagnet $CeIr_3Si_2$, Phys. Rev. B Condens. Matter (2007) 184429 (1-6).
[39] STOE WINXPOW (Version 1.06), Stoe & Cie GmbH, Darmstadt, Germany, 1999.
[40] J. Rodriguez-Carvajal, Abstracts of the Satellite Meeting on Powder Diffraction of the XV Congress of the IUCr, Toulouse, France, 1990, p. 127. Book of.
[41] T. Roisnel, J. Rodriguez-Carvajal, in: Proceedings of the European Powder Diffraction Conference (EPDIC7), Materials Science Forum, 2000, p. 118. Book of.
[42] http://materials.springer.com/.
[43] H. Okamoto, The Ce-Ir (Cerium-Iridium) system, J. Phase Equilib. 12 (1991) 563–565.
[44] V.N. Dmitrieva, T. Resukhina, L. Varekha, L. Kravchenko, V. Vorob'ev, B. Gusienin, V. Domashev, V. Melnikova, Phase diagram and thermodynamic properties of a number of intermetallic compounds of the iridium-cerium system, Metallofizika 49 (1973) 109–117 (in Russian).
[45] G.L. Olcese, Crystal structure and magnetic properties of some 7:3 binary phases between lanthanides and metals of the 8th group, J. Less-Common Met. 33 (1973) 71–81.
[46] Z. Blazina, R.C. Mohanty, A. Raman, Intermediate phases in some rare-earth-metal – iridium systems, Z. Met. 80 (1989) 192–196.
[47] J.M. Moreau, D. Paccard, J. Le Roy, Cerium-iridium Ce_5Ir_3 and Ce_5Ir_4, Acta Cryst. B 36 (1980) 912–914.
[48] M.V. Bulanova, P.N. Zheltov, K.A. Meleshevich, P.A. Saltykov, G. Effenberg, Cerium – silicon system, J. Alloys Compd. 345 (2002) 110–115.
[49] P. Schobinger-Papamantellos, K.H.J. Buschow, Two-step ferromagnetic ordering of $Ce_2Si_{3-\delta}$, J. Alloys Compd. 198 (1993) 47–50.
[50] H. Okamoto, Comment on Ir – Si (iridium – silicon), J. Phase Equilib. 16 (1995) 473.
[51] H. Okamoto, Ir – Si (iridium – silicon), J. Phase Equilib. Diffus. 28 (2007), 495–495.
[52] C.E. Allevato, C.B. Vining, Phase diagram and electrical behavior of silicon-rich iridium silicide compounds, J. Alloys Compd. 200 (1993) 99–105.
[53] J.B. Sha, Y. Yamabe-Mitarai, Phase and microstructural evolution of Ir – Si binary alloys with fcc/silicide structure, Intermetallics 14 (2006) 672–684.
[54] I. Engström, E. Zdansky, Polymorphism in $IrSi_3$, Acta Chem. Scand. A 36 (1982) 857–858.
[55] S. Bhan, K. Schubert, Zum Aufbau der System Kobalt-Germanium, Rhodium-Silizium sowie einiger verwandten Legierungen, Z. Met. 51 (1960) 327–329.
[56] L.N. Finnie, Structures and compositions of the silicides of ruthenium, osmium, rhodium and iridium, J. Less-Common Met. 4 (1962) 24–34.
[57] I. Engström, F. Zackrisson, X-ray studies of silicon-rich iridium silicides, Acta Chem. Scand. 24 (1970) 2109–2116.
[58] J.G. White, E.F. Hockings, Crystal structure of iridium trisilicide, $IrSi_3$, Inorg. Chem. 10 (1971) 1934–1935.
[59] J. Emsley, The Elements, Oxford University Press, Oxford (UK), 1999.
[60] E. Parthé, L. Gelato, B. Chabot, M. Penzo, K. Cenzual, R. Gladyshevskii, TYPIX Standardized Data and Crystal Chemical Characterization of Inorganic Structure Types, Springer-Verlag, Berlin, Heidelberg, 1994.
[61] A.I. Tursina, A.V. Gribanov, Y.D. Seropegin, O.I. Bodak, Crystal structures of the ternary cerium rhodium silicides $Ce_2Rh_{12}Si_7$ and $Ce_6Rh_{30}Si_{19}$, J. Alloys Compd. 367 (2004) 142–145.
[62] R. Mishra, R.-D. Hoffmann, R. Pöttgen, Two- and three-dimensional [IrSi] networks in the silicides $Sm_3Ir_2Si_2$, HoIrSi, and YbIrSi, Z. Anorg. Allg. Chem. 627 (2001) 1787–1792.
[63] Y.M. Prots, J. Stepien-Damm, P.S. Salamakha, O.I. Bodak, The crystal structure of orthorhombic $Ce_3Rh_3Si_2$, an intergrowth of FeB- and YPd_2Si-type slabs, J. Alloys Compd. 256 (1997) 166–169.
[64] T.B. Massalski, H. Okamoto, P.R. Subramanian, L. Kacprzak, Binary Alloy Phase Diagrams, ASM International, Materials Park, OH, USA, 1990.
[65] M. Ellner, K. Kolatschek, B. Predel, On the partial atomic volume and the partial molar enthalpy of aluminium in some phases with Cu and Cu_3Au structures, J. Less- Common Met. 170 (1991) 171–184.
[66] F. Weitzer, J.C. Schuster, J. Bauer, B. Jounel, Phase equilibria in ternary RE-Si-N systems (RE=Sc, Ce, Ho), J. Mater. Sci. 26 (1991) 2076–2080.
[67] I.R. Mokra, O.I. Bodak, E.I. Gladyshevskii, The cerium-neodymium-silicon system, dopovidi akademii Nauk Ukrains'koi RSR, Seriya A Fiziko-Mat. Tekh. Nauk. (1978) 1043–1045 (in Ukrainian).
[68] A. Raman, Crystal structure of Ce_5Rh_4 and analogous phases, J. Less-Common Met. 48 (1976) 111–117.
[69] V.D. Vorob'ev, V.A. Melnikova, X-ray study of the systems Iridium-Lanthanum and Iridium-Cerium, Kristallografiya 19 (1974) 397.
[70] O. Sologub, P. Salamakha, A.P. Gonçalves, H. Ipser, M. Almeida, Crystal structure of the $CeIr_3$ compound, J. Alloys Compd. 373 (2004) L5–L7.
[71] G. Kimmel, On the U_3Si (Doc) crystallographic type, J. Less-Common Met. 59 (1978) 83–86.
[72] M. Ellner, B. Predel, Durch extrem rasche abkühlung von schmelzen erzielbare phasen in den systemen Ni-Ge, Pd-Ge und Pt-Ge, J. Less-Comm. Met. 76 (1980) 181–197.
[73] K. Schubert, S. Bhan, W. Burkhardt, R. Gohle, H.G. Meissner, M. Pötzschke, E. Stolz, Einige strukturelle Ergebnisse an metallischen phasen (5), Naturwissenschaften 47 (1960), 303–303.
[74] I. Engström, T. Lindsten, E. Zdansky, The crystal structure of the iridium silicide Ir_3Si_5, Acta Chem. Scand. 41A (1987) 237–242.
[75] A. Verniere, P. Lejay, P. Bordet, J. Chenavas, J.L. Tholence, J.X. Boucherle, N. Keller, Crystal structure and physical properties of new ternary silicides $R_4T_{13}X_9$ (R, rare earth or uranium; T, rhodium or iridium; X, silicon or germanium), J. Alloys Compd. 218 (1995) 197–203.